The Spectroscopy of $HMn(CO)_5$: A CASSCF/MRCI and CASPT2 ab Initio Study

Michel R. J. Hachey[†] and Chantal Daniel*

Laboratoire de Chimie Quantique, UPR 139 du CNRS, Université Louis Pasteur, Institut Le Bel 4, Rue Blaise Pascal, F67000 Strasbourg Cedex, France

Received June 17, 1997

The electronic structure of the states of $HMn(CO)_5$ in the near-UV region was investigated by CASSCF/MRCI and CASPT2 ab initio methods with a basis set between double- and triple-ζ quality including very diffuse functions. On the basis of calculated vertical excitation energies and oscillator strengths, the following absorption band assignments could be made: (1) A^1E ($3d_\pi \rightarrow 3d_{x^2-y^2}$) and B^1E ($3d_\pi \rightarrow \sigma^*_{Mn-H}$) transitions underlie the low-intensity shoulder at 229 nm; (2) the high-intensity B^1A_1 ($3d_\pi \rightarrow \pi^*_{CO,12e} + 3d_{xy} \rightarrow \pi^*_{CO,3b_2}$) and weak C^1E ($3d_\pi \rightarrow \pi^*_{CO,3b_2}$) transitions underlie the central band at 214 nm; and (3) the very high intensity C^1A_1 ($\sigma_{Mn-H} \rightarrow \sigma^*_{Mn-H}$) underlies mainly the band at 193 nm. This identifies the most likely photoinitiating states for the photochemistry of $HMn(CO)_5$. The a^3A_1 was shown to have valence character, contrary to previous suggestions.

1. Introduction

Transition-metal hydride complexes are characterized in the visible near-UV region by their high density of states within rather narrow domains of energy. This makes the acquisition of fine structure for excited states improbable or at least difficult, hampering a strictly experimental determination of the photoactive states responsible for the observed primary reactions. From the theoretical side, the high density of states causes severe correlation effects that require careful calculations able to describe the correlation in different electronic states in a balanced way. One of the simplest and best studied transition-metal hydrides is $HMn(CO)_5$. The spectroscopy and photochemistry of this prototype molecule have been the subject to several experimental investigations[1−3] and high-level theoretical studies,[4,5] but still much work needs to be done. Recent studies of the photochemistry of $ClMn(CO)_5$ and $Mn_2(CO)_{10}$, based on the density functional theory,[6,7] have pointed to the importance of the theoretical approach in the understanding of the primary reaction mechanisms. The computation of the potential energy curves corresponding to the carbonyl loss, and to the homolysis in this family of molecules, has enabled the authors to propose comparative mechanisms of photodissociation of $RMn(CO)_5$ (R = H, Cl) and $Mn_2(CO)_{10}$.

Under irradiation at 193 nm, two primary competing photodissociation processes are observed in matrixes.[2] The major photodissociation event is a heterolytic carbonyl ligand loss,

$$HMn(CO)_5 \xrightarrow{h\nu} HMn(CO)_4 + CO \qquad (1)$$

and the minor competing reaction corresponds to a metal hydride bond homolysis,

$$HMn(CO)_5 \xrightarrow{h\nu} Mn(CO)_5 + H \qquad (2)$$

At a lower irradiation energy of 229 nm, the metal carbonyl heterolysis of reaction 1 is still observed, but evidence for Mn−H homolysis in reaction 2 essentially disappears.[2]

The experimental findings are not sufficient to establish with certainty the nature of the photoactive states and the photodissociation mechanism. The absorption spectrum recorded in the vapor phase shows two intense overlapping bands at 195 (51 300 cm^{-1}) and 214 nm (46 730 cm^{-1}) and a low-intensity shoulder in the lower part of the spectrum at around 290 nm (34 500 cm^{-1}). It is uncertain how many transitions underlie these broad and rovibrationally structureless bands. On energetic grounds, the photoinitiating state for reaction 1 should underlie the weak shoulder at 290 nm, and for reaction 2 it should underlie the intense upper bands near 200 nm.

In a previous theoretical study,[5] a qualitative mechanism based on CASSCF/CCI potential energy curves has been proposed for reactions 1 and 2. The heterolytic loss of an axial carbonyl ligand (1) occurs along the dissociative ^1E ($3d_\pi \rightarrow \sigma^*$) potential energy curve. The proposed mechanism for the metal hydride homolysis (2) begins with an absorption to ^1E ($3d_\pi,\pi^*$) followed by a radiationless transition to $^3A_1$ (σ,σ^*), which dissociates to the diradicals H and $Mn(CO)_5$ in their ground states ($^{1,3}A_1$ dissociation channel). The $^3A_1$ ($\sigma \rightarrow \sigma^*$) transition, lying much higher than ^1E ($3d_\pi \rightarrow \pi^*$), qualitatively reproduces the energy dependence of the photoreactivity, namely, quenching of the homolysis at lower irradiation energy. However, recent studies of the photodissociation dynamics in transition-metal hydrides and dihydrides do not seem to support this mechanism. Wave packet propagation on spin−orbit-coupled potentials in related complexes suggests that the intersystem crossing processes are not competitive with faster direct dissociation on singlet states.[8,9]

A question left from previous theoretical studies is the nature of the a^3A_1 state.[4,5] This has a large influence on the dissociative

[†] Present address: University of New Brunswick, Fredericton, Canada.

(1) Blakney, G. B.; Allen, W. F. *Inorg. Chem.* **1971**, *10*, 2763.
(2) Church, S. P.; Poliakoff, M.; Timney, J. A.; Turner, J. J. *Inorg. Chem.* **1983**, *22*, 3259.
(3) Church, S. P.; Poliakoff, M.; Timney, J. A.; Turner, J. J. *J. Am. Chem. Soc.* **1981**, *103*, 7515.
(4) Veillard, A.; Strich, A.; Daniel, C.; Siegbahn, P. E. M. *Chem. Phys. Lett.* **1987**, *141*, 329.
(5) Daniel, C. *J. Am. Chem. Soc.* **1992**, *114*, 1625.
(6) Wilms, M. P.; Baerends, E. J.; Rosa, A.; Stufkens, D. J. *Inorg. Chem.* **1997**, *36*, 1541.
(7) Rosa, A.; Ricciardi, G.; Baerends, E. J.; Stufkens, D. J. *Inorg. Chem.* **1995**, *34*, 3425. Rosa, A.; Ricciardi, G.; Baerends, E. J.; Stufkens, D. J. *Inorg. Chem.* **1996**, *35*, 2886.
(8) Daniel, C.; Heitz, M. C.; Manz, J.; Ribbing, C. *J. Chem. Phys.* **1995**, *102*, 905.
(9) Heitz, M. C.; Ribbing, C.; Daniel, C. *J. Chem. Phys.* **1997**, *106*, 1421.

S0020-1669(97)00752-0 CCC: $15.00
Published on Web 02/28/1998

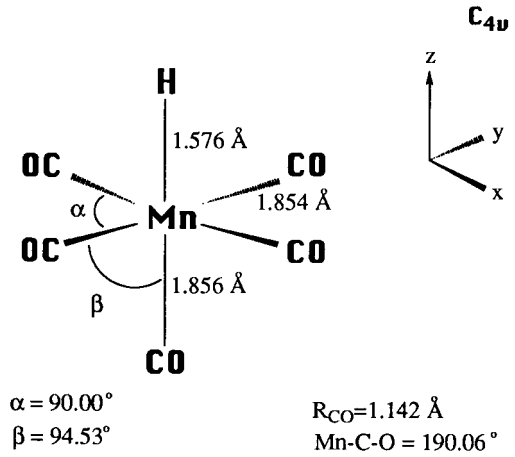

Figure 1. Experimental structure of $HMn(CO)_5$.[12]

$b^3A_1(\sigma,\sigma^*)$ state through the presence of an avoided crossing along the Mn−H elongation potential curve. While earlier basis sets did not implicitly include Rydberg diffuse exponents, the results nonetheless suggest the assignment of a^3A_1 to the $3d_{xy} \rightarrow 4d_{xy}$ Rydberg transition, where the $4d_{xy}$ orbital has a non-negligible π^* contribution. This issue warrants further investigation.

Assignments of the UV bands have relied heavily on theoretical calculations, but several of the charge-transfer states in the photoactive energy region have not yet been evaluated because of the emphasis on the $d \rightarrow \sigma^*$, $\sigma \rightarrow \sigma^*$, and metal-centered excitations, which hold the key to the photochemical behavior. To date, only the lowest $d \rightarrow d$ transition band at 290 nm has been assigned with rigor on the basis of ab initio results,[4,5,10] confirming an earlier controversial reassignment.[1,11] Only suggestions were given toward the nature of the more intense metal-to-ligand charge-transfer (MLCT) bands lying at higher energies.

The present theoretical study aims to better determine which states may contribute to the absorption spectrum of $HMn(CO)_5$. The move toward a more quantitative dynamic simulation requires a more rigorous characterization of states involved in the photochemical process. Since irradiation between 190 and 230 nm is used in the photolysis of $HMn(CO)_5$, characterization of photophysical properties of states over this visible/UV region will be given. To address the question of the Rydberg nature of the a^3A_1 state, a basis set with sufficient flexibility to explicitly describe the Rydberg orbitals will be used. Since the 4s and 4p orbitals should lie below the 4d orbital, the above a^3A_1 assignment implies that the $3d_{xy} \rightarrow$ 4s and 4p transitions should also lie in the photoactive region. While it is unlikely that Rydberg states would take part directly in the photochemistry, one cannot discount an auxiliary role that could be of importance in internal conversion processes, for example.

A comparison of MRCI and CASPT2 energies obtained with the parent CASSCF wave functions will be given. Many of the states involved are to a zeroth approximation better described by a multideterminantal wave function as opposed to a single determinantal representation.

2. Computational Methods

The calculations on $HMn(CO)_5$ (Figure 1) were carried out starting from the experimental geometry of McNeill and Scholer[12] in order to be consistent with previous calculations. This geometry is very close to the more refined microwave structure proposed recently by Kucholich et al.[13] The following basis sets were used: for the manganese atom a (15,11,6) primitive set contracted to [9,6,3],[14,15] and further augmented—to describe the Rydberg states—with two sets of diffuse functions (α_s = 0.014, 0.0046; α_p = 0.030, 0.010; α_d = 0.037, 0.013 with contraction coefficients of 1); for first-row atoms (10,6) sets contracted to [4,2];[16] and for hydrogen (6,1)/[3,1].[17] This basis set is triple-ζ for the 1s shell of hydrogen and for the 3d and 4s shells of the metal; otherwise it is double-ζ. For the sake of comparison, some calculations have been performed using generally contracted atomic natural orbitals (ANO).

The $^1A_1$ ground-state electronic configuration of $HMn(CO)_5$ conforms to a closed-shell occupation of $(1a_2)(6b_1)(17a_1)(2b_2)(11e)$, corresponding to the $(\pi_{CO})^2(\pi_{CO})^2(\sigma_{Mn-H})^2(3d_{xy})^2(3d_\pi)^4$ electronic configuration. Low-lying virtual orbitals correspond to $3d_{x^2-y^2}(7b_1)$, $\sigma^*_{Mn-H}(18a_1)$, and π^*_{CO} (12e, $3b_2$).

The calculations have been carried out in C_{2v} symmetry, but the supersymmetry option has been used to maintain degeneracy properties of the C_{4v} point group. CASSCF wave functions used in subsequent CASPT2 and MRCI calculations were calculated in various ways: (1) optimized individually for each state of interest ("parent" wave function); (2) averaged over several roots of a given symmetry; and to corroborate previous work (3) with $^5A_2$ state CASSCF reference wave function. Eight electrons were correlated in 11 active orbitals including σ_{Mn-H} ($17a_1$), σ^*_{Mn-H} ($18a_1$), $3d_\pi$ (11e), and $3d_\delta$ ($2b_2$, $7b_1$) orbitals with the $3d'/\pi^*_{co}$ ($3b_2$, 12e) orbitals of correlation. Two extra virtual orbitals, $4b_2$ and $5b_2$ (in C_{4v}), were also kept active to localize the 4d Rydberg orbital and one of the π^* orbitals; however, these higher virtual orbitals turned out to have negligible occupation numbers of at most 0.002 to a low of 0.0001 in the ground and exited states studied. Because CASSCF wave functions give a reasonable account of the nondynamical correlation effects, they constitute a good starting point for the addition of more extensive correlation by MRCI or CASPT2 treatments.

The following technical details are to be noted for the MRCI or CASPT2 calculations. The 15 lowest core orbitals ($9a_1$, $3b_1$, and $3b_2$) (in C_{2v}) were frozen, and their complementary 15 highest molecular orbitals (MOs) were discarded. All valence electrons were correlated in the CASPT2 calculations. For the CI treatments, low-lying valence orbitals ($13a_1$, $7b_1$, $7b_2$, and $2a_2$) (in C_{2v}) were frozen in addition to those of the core orbitals. The same eight electrons as in the CASSCF wave function were correlated at the CI level using 10 to 20 reference configurations. Single and double excitations to all virtual orbitals except for those that were discarded (highest orbital counterparts to the carbonyl 1s and metal 1s, 2s, and 2p) were performed.

The calculations were carried out using the Molcas-3 suite of programs.[18]

3. Results

The vertical excitation energies obtained by different methods of calculation are reported in Table 1, along with contracted CI literature values for comparison.[4,5] The main CI coefficients of the excited states are also given in Table 1 and illustrate well the significant amount of mixing between states. The energetic ordering in the Franck−Condon region is indicated alphabetically (in capitals for the singlet states and in small

(10) Eyermann, C. J.; Chung-Phillips, A. *J. Am. Chem. Soc.* **1984**, *106*, 7437.
(11) McLean, R. A. N. *J. Chem. Soc., Dalton Trans.* **1974**, 1568.
(12) McNeill, E. A.; Scholer, F. R. *J. Am. Chem. Soc.* **1977**, *99*, 6243.
(13) Kukolich, S. G.; Sickafoose, S. M. *Inorg. Chem.* **1994**, *33*, 1217.
(14) Wachters, A. J. H. *J. Chem. Phys.* **1970**, *52*, 1033.
(15) (a) The 14s9p5d primitive set of Wachter's was expanded by an additional s function (exponent 0.2735), d diffuse exponents, and two diffuse p by the even-tempered criterion of Raffeneti. (b) Raffenetti, R. C.; Bardo, R. D.; Ruedenberg, K. In *Energy Structure and Reactivity*; Smith, D. W., McRae, W. B., Eds.; Wiley: New York, 1973; p 164.
(16) Huzinaga, S. *Approximate Atomic Functions*; Technical Report, University of Alberta: Alberta, Canada, 1971.
(17) Huzinaga, S. *J. Chem. Phys.* **1965**, *42*, 1293.
(18) Andersson, K.; Blomberg, M. R. A.; Fülscher, M. P.; Kellö, V.; Lindh, R.; Malmqvist, P.-Å.; Noga, J.; Olsen, J.; Roos, B. O.; Sadlej, A. J.; Siegbahn, P. E. M.; Urban, M.; Widmark, P.-O. *Molcas version 3*; University of Lund: Sweden, 1994.

Table 1. Calculated MRCI (Based on Either Average CASSCF (MO) or CASSCF Natural Orbitals (NO) Optimized for the State of Interest) and CASPT2 Excitation Energies (in cm^{-1}) for the Electronic Excited States[a]

	one-electron excitation in the principal configurations	MRCI/MO	MRCI/NO	CASPT2	CCI(D92)[b]	CCI(VSDS87)[c]
$^1A_1 \rightarrow a^3E$	$3d_\pi \rightarrow 3d_{x^2-y^2}$ (0.89)	27 100	26 500	27 300	23 940	25 200
$^1A_1 \rightarrow a^3A_2$	$3d_{xy} \rightarrow 3d_{x^2-y^2}$ (0.91)	28 300	28 100	28 800	26 800	27 600
$^1A_1 \rightarrow b^3E$	$3d_\pi \rightarrow \sigma^*_{Mn-H}$ (0.87)	34 500	34 500	31 700	32 940	
	$3d_\pi \rightarrow 3d_{x^2-y^2}$ (−0.24)					
$^1A_1 \rightarrow A^1A_2$	$3d_{xy} \rightarrow 3d_{x^2-y^2}$ (0.92)	35 200	34 600	35 300	33 800	33 300
$^1A_1 \rightarrow a^3A_1$	$3d_{xy} \rightarrow \pi^*_{CO,3b_2}$ (0.50)	35 800[d]	35 400			
	$3d_\pi \rightarrow \pi^*_{CO,12e;b_1}$ (−0.52)					
	$3d_\pi \rightarrow \pi^*_{CO,12e;b_2}$ (0.52)					
$^1A_1 \rightarrow A^1E$	$3d_\pi \rightarrow 3d_{x^2-y^2}$ (0.86)	36 100	35 600	34 200	33 580	33 700
	$3d_\pi \rightarrow \sigma^*_{Mn-H}$ (0.30)					
$^1A_1 \rightarrow a^3B_2$	$3d_{xy} \rightarrow \sigma^*_{Mn-H}$ (0.90)	39 500	39 500	36 500[e]		
$^1A_1 \rightarrow c^3E$	$3d_\pi \rightarrow \pi^*_{CO,3b_2}$ (0.90)	40 000	40 000			
$^1A_1 \rightarrow a^3B_1$	$3d_\pi \rightarrow \pi^*_{CO,12e;b_1}$ (0.62)	41 400[d]	40 500			
	$3d_\pi \rightarrow \pi^*_{CO,12e;b_2}$ (0.63)					
$^1A_1 \rightarrow b^3A_1$	$3d_{xy} \rightarrow \pi^*_{CO,3b_2}$ (0.74)	41 700[d]			38 230	
	$3d_\pi \rightarrow \pi^*_{CO,12e;b_1}$ (0.36)					
	$3d_\pi \rightarrow \pi^*_{CO,12e;b_2}$ (−0.34)					
$^1A_1 \rightarrow B^1E$	$3d_\pi \rightarrow \sigma^*_{Mn-H}$ (0.68)	42 100[d]	41 400	42 000[e]	43 150	42 300
	$3d_\pi \rightarrow \pi^*_{CO,3b_2}$ (−0.48)					
	$3d_\pi \rightarrow 3d_{x^2-y^2}$ (−0.31)					
$^1A_1 \rightarrow A^1B_2$	$3d_{xy} \rightarrow \sigma^*_{Mn-H}$ (0.76)	45 700		42 900[e]		
	$3d_\pi \rightarrow \pi^*_{CO,12e;b_1}$ (0.28)					
	$3d_\pi \rightarrow \pi^*_{CO,12e;b_2}$ (0.28)					
$^1A_1 \rightarrow C^1E$	$3d_\pi \rightarrow \pi^*_{CO,3b_2}$ (0.77)	47 500[d]				
	$3d_\pi \rightarrow \sigma^*_{Mn-H}$ (0.33)					
	$3d_\pi \rightarrow 3d_{x^2-y^2}$ (−0.21)					
$^1A_1 \rightarrow A^1B_1$	$3d_\pi \rightarrow \pi^*_{CO,12e;b_1}$ (−0.50)	48 400[d]				
	$3d_\pi \rightarrow \pi^*_{CO,12e;b_2}$ (−0.50)					
	$\sigma_{Mn-H} \rightarrow 3d_{x^2-y^2}$ (0.43)					
$^1A_1 \rightarrow c^3A_1$	$\sigma_{Mn-H} \rightarrow \sigma^*_{Mn-H}$ (0.86)	48 900[d]				46 900
$^1A_1 \rightarrow B^1A_1$	$3d_{xy} \rightarrow \pi^*_{CO,3b_2}$ (0.65)	49 700[d]			50 700	49 000
	$3d_\pi \rightarrow \pi^*_{CO,12e;b_1}$ (0.39)					
	$3d_\pi \rightarrow \pi^*_{CO,12e;b_2}$ (−0.39)					
$^1A_1 \rightarrow b^3B_1$	$\sigma_{Mn-H} \rightarrow 3d_{x^2-y^2}$ (0.85)	51 200[d]				
$^1A_1 \rightarrow B^1B_1$	$\sigma_{Mn-H} \rightarrow 3d_{x^2-y^2}$ (0.73)	53 000[d]				
	$3d_\pi \rightarrow \pi^*_{CO,12e;b_1}$ (0.21)					
	$3d_\pi \rightarrow \pi^*_{CO,12e;b_2}$ (0.21)					
$^1A_1 \rightarrow C^1A_1$	$\sigma_{Mn-H} \rightarrow \sigma^*_{Mn-H}$ (−0.62)	55 000[d]			65 800	61 800
	$3d_{xy} \rightarrow \pi^*_{CO,12e;b_1}$ (−0.23)					

[a] CASSCF wave function averaged over the first states (3 to 5) of a given spin and symmetry with equal weights. [b] From ref 5. [c] From ref 4. [d] The ground state MRCI energies were −1 713.818 334 au with the parent wave function and −1 713.822 077 au for the average CASSCF. [e] CASPT2 energy with level shift of 0.05 to discount intruder states. Ground-state energy including level shift corrections is −1 715.097 488 au.

letters for the triplet states). Attempts were made to optimize the CASSCF wave functions (molecular orbitals used in the subsequent MRCI treatment are denoted NO) individually for all states; however near degeneracies among configurations of the same symmetry species often caused convergence problems at the CASSCF level and/or at the MRCI levels. For most states above 35 000 cm^{-1}, it became necessary to use the CASSCF MOs averaged over several states rather than those of the parent wave function.

The high degree of mixing in the high-lying states caused a CASPT2 intruder-state problem. Attempts at removing the intruder states by including shift corrections[19] of 0.02 and 0.2 hartrees had marginal success in some cases but for the most part failed to remove the intruder-state contamination. The active space could not be increased easily to resolve this problem, as the number of intruder states involved requires an active space that exceeds current program limitations.

3.1. Excited States between 180 and 380 nm. This work identifies at least 19 states underlying the $HMn(CO)_5$ electronic spectrum between 27 000 and 55 000 cm^{-1}, that is, 369 and 181 nm. We find four low-lying states of predominantly metal centered, d → d type, transitions. The lowest singlet excited states correspond to A^1A_2 ($3d_{xy} \rightarrow 3d_{x^2-y^2}$) at 35 200 cm^{-1} and A^1E ($3d_\pi \rightarrow 3d_{x^2-y^2}$) at 36 100 cm^{-1}. Their triplet counterparts, a^3A_2 ($3d_{xy} \rightarrow 3d_{x^2-y^2}$) and a^3E ($3d_\pi \rightarrow 3d_{x^2-y^2}$), are calculated at 28 300 and 27 100 cm^{-1}, respectively.

Just above, four states are computed that correspond predominantly to d → σ^* excitations. The B^1E ($3d_\pi \rightarrow \sigma^*_{Mn-H}$) transition at 42 100 cm^{-1} shows a large contribution from $3d_\pi,\pi^*_{CO}$ ($3b_2$), whereas the corresponding b^3E triplet state at 34 500 cm^{-1} is nearly pure $3d_\pi,\sigma^*_{Mn-H}$. Similarly, the A^1B_2 ($3d_{xy} \rightarrow \sigma^*_{Mn-H}$) at 45 700 cm^{-1} also has a large $3d_\pi,\pi^*_{CO}$ (12e) contribution, while the a^3B_2 triplet state at 39 500 cm^{-1} is essentially pure.

As indicated in the Introduction, the $\sigma_{Mn-H} \rightarrow \sigma^*_{Mn-H}$ excitation plays an important role in the metal−hydrogen bond homolysis reactions of several transition-metal hydrides.[20] The c^3A_1 ($\sigma_{Mn-H},\sigma^*_{Mn-H}$) state is calculated at 48 900 cm^{-1} vertically. Its potential is known to be dissociative for Mn−H bond elongation.[5] The corresponding C^1A_1 ($\sigma_{Mn-H} \rightarrow \sigma^*_{Mn-H}$) is found at about 55 000 cm^{-1}, but unlike its purer triplet

(19) Roos, B. O.; Andersson, K. *Chem. Phys. Lett.* **1995**, *245*, 215.

(20) Daniel, C.; Veillard, A. In *Transition Metal Hydrides*; Dedieu, A., Ed.; VCH Publisher: New York, 1991; p 235.

Table 2. Oscillator Strengths (f), Transition Dipole Moments (μ), and Relative Intensities for Symmetry- and Spin-Allowed Transitions of $HMn(CO)_5$ and Comparisons to Measured Absorption Spectrum Values[a]

	energies (cm^{-1})	μ (au)	f	intens rel[b]
band I	**34 500**			2
A^1E	36 100	−0.254	0.0060	1.1
B^1E	42 100	−0.147	0.0023	0.4
band II	**46 730**			15
C^1E	47 500	−0.163	0.0038	0.7
B^1A_1	49 700	−0.703	0.0750	14.3
band III	**51 300**			20
C^1A_1	∼55 000	−1.489	0.3724	71.3

[a] Experimental vapor phase values of Blakney and Allen[1] are given in boldface. [b] Calculated relative intensity is given with respect to the sum of the oscillator strengths for transitions to C^1E and B^1A_1.

counterpart, it shows very heavy mixing with configurations such as ($3d_\pi$,π^*_{CO} (12e)), ($3d_{xy}$,π^*_{CO} ($3b_2$)) and with several small but numerous double-excitation contributions. The C^1A_1 state is interpreted as the first $^1A_1$ wave function having a significant $\sigma_{Mn-H} \rightarrow \sigma^*_{Mn-H}$ contribution (about 40% of the weight). The remaining 60% of the σ_{Mn-H},σ^*_{Mn-H} configuration contributions still remains to be accounted for in higher $^1A_1$ excited sates. This explains the discrepancy of 6800 cm^{-1} with the previously reported $^1(\sigma_{Mn-H} \rightarrow \sigma^*_{Mn-H})$ transition, which very likely has optimized on a higher state also having a significant σ_{Mn-H},σ^*_{Mn-H} contribution.

The B^1B_1 and b^3B_1 ($\sigma_{Mn-H} \rightarrow 3d_{x^2-y^2}$) lie very close to one another at 51 200 and 53 000 cm^{-1}, respectively. The energy gap of 1800 cm^{-1} between the two is the smallest among singlet−triplet pairs. Because these are symmetry forbidden transitions and since they cannot couple vibronically to intense $^1A_1 \rightarrow {}^1A_1$ transitions lying nearby, the $\sigma_{Mn-H} \rightarrow 3d_{x^2-y^2}$ transitions are not expected to play important roles in the spectroscopy or in the photochemistry.

Finally, we describe the states generated by the $3d \rightarrow \pi^*_{CO}$ MLCT transitions. Despite their π^*_{CO} denomination, these orbitals show a significant contribution of the 3d′ of correlation whatever the basis set used (see Results section 3.3). On the basis of the π^*_{CO} orbital relative energies, the calculation has been restricted to the states generated by the π^*_{CO} (b_2) and the π^*_{CO} (12e) orbitals (oriented out of the *xy* plane). Three $3d_\pi \rightarrow \pi^*_{CO}$ transitions were calculated: a^3A_1 at 35 800 cm^{-1}, a^3B_1 at 41 400 cm^{-1}, and c^3E at 40 000 cm^{-1}, corresponding to two transitions to π^*_{CO} (12e) and one to π^*_{CO} ($3b_2$), respectively. While the a^3B_1 and c^3E states are relatively pure, the a^3A_1 state shows considerable mixing between the $3d_\pi$,π^*_{CO} (12e) and $3d_{xy}$,π^*_{CO} ($3b_2$) configurations. Note, the mixed nature of the a^3A_1 wave function is especially poorly reproduced by using the parent CASSCF wave function, yielding a mediocre MRCI wave function (despite a generous set of references) and causing insurmountable problems in the CASPT2 results. The corresponding C^1E, A^1B_1, and B^1A_1 singlet states are found at 47 500, 48 400, and 49 700 cm^{-1}, respectively, and all show much more mixed compositions compared to their triplet counterparts.

3.2. Intensity of Spin- and Symmetry-Allowed Transitions. The transition dipole moments, oscillator strengths, and relative intensities of symmetry- and spin-allowed transitions, calculated at the CASSCF level, are reported in Table 2 and are compared to the recorded absorption spectrum in the vapor phase for which relative intensities of the three main bands are available. In this work, relative intensities were calculated with respect to the sum of the B^1A_1 ($3d_{xy} \rightarrow \pi^*_{CO}$ ($3b_2$)) and C^1E ($3d_\pi \rightarrow \pi^*_{CO}$ ($3b_2$)) oscillator strengths, which corresponds best to the central high-intensity absorption band at 214 nm (46 730 cm^{-1}; band II).

Energetically, the A^1E ($3d_\pi \rightarrow 3d_{x^2-y^2}$) and B^1E ($3d_\pi \rightarrow \sigma^*_{Mn-H}$) excited states underlie the shoulder at 229 nm (34 500 cm^{-1}; band I), and their oscillator strengths are weak in agreement with experiment. The $A^1E \leftarrow {}^1A_1$ absorption is about three times more intense than the $B^1E \leftarrow {}^1A_1$ absorption.

Most of the intensity of the central absorption band (band II) comes from the $B^1A_1 \leftarrow {}^1A_1$ absorption which is calculated to be about 20 times stronger than the $C^1E \leftarrow {}^1A_1$ absorption intensity. Note that both of these MLCT states are characterized by large mixing with other states, as illustrated by the coefficients of Table 1.

The $^1A_1 \rightarrow C^1A_1$ transition gives the biggest calculated oscillator strength and, thus, should give rise to one of the more intense features of the spectrum. It provides a good match to the highest intensity band in the spectrum (51 300 cm^{-1}; band III). The C^1A_1 ($\sigma_{Mn-H} \rightarrow \sigma^*_{Mn-H}$) excitation is expected to lead to a significant Mn−H elongation in the excited state relative to the ground state; therefore the resulting band is expected to be very broad. It is to be remembered that this state has a highly mixed character so that the $\sigma_{Mn-H} \rightarrow \sigma^*_{Mn-H}$ assignment is a bit ambiguous in the vertical region; however, regardless of the label used, it is clear that transition to this state has a strong intensity contribution to the spectrum.

3.3. The Nature of the a^3A_1 and b^3A_1 States. As seen in section 3.2, the state labeled as a^3A_1 in previous work is shown in this study to actually correspond to the second state of this space and spin symmetry, that is, b^3A_1. The convergence on the second state is due to a bias of the CASSCF wave function optimized for a unique state which favors a single-determinant description. The mixed composition of the CI wave function demonstrates that the relatively pure composition of the single CASSCF root solution is insufficient and recommends the use of the CASSCF wave function average over several states.

The extended basis set in the present work is sufficiently flexible to describe the first Rydberg states. The b^3A_1 wave function suggests a $3d_{xy} \rightarrow \pi^*_{CO}$ ($3b_2$) assignment rather than a Rydberg characterization previously suggested. Indeed, careful analysis of the $3b_2$ orbital indicates that this orbital is predominantly of π^*_{CO} character, although mixed with the $3d'_{xy}$ which correlates $3d_{xy}$. The valence nature of this orbital is validated by the total electronic $\langle r^2 \rangle$ expectation value of −1820, −1822, and −1822 au for the ground and a,b^3A_1 states, respectively. This shows that both the a^3A_1 and b^3A_1 states are as compact as the ground state. Other valence states also have $\langle r^2 \rangle$ values around −1820 au, as expected. Interestingly, the large π^* ligand contribution to the $3b_2$ MO does not appear fortuitous and actually increases in the approximate orbital obtained with CASPT2.

The CASSCF $\langle r^2 \rangle$ expectation values for Rydberg states could only be obtained with a constrained active space: 8 electrons in the highest $1a_1$, $1b_1$, $1b_2$, and $1a_2$ occupied orbitals and 4 additional a_2 virtuals (in C_{2v}). This active space gives a valence b^3A_1 ($3d_{xy}$,π^*_{CO}) value of −1809 au, while the more extended $^1B_2$ ($3d_\pi \rightarrow 5d_{xy}$) and $^{1,3}A_1$ ($3d_{xy} \rightarrow 5d_{xy}$) Rydberg excited states show, as expected, significantly larger $\langle r^2 \rangle$ values of −1927, −1903, and −1922 au, respectively. Energetically, the CASSCF results place the first singlet Rydberg states at around 67 000 cm^{-1}. The MRCI energies could not be obtained due to convergence problems, but a stabilization due to correlation by about 10 000 cm^{-1} is estimated. This value corresponds to the usual lowering of the excitation energy on going from the CASSCF level to the MRCI level. This is in keeping with the

experimental estimate of 58 400 cm^{-1}, which one gets from the molecular IP (71 380 cm^{-1})[21] and an atomic term value of 12 960 cm^{-1}.[22]

Calculations carried out with the small ANO basis from Molcas-3, contracted to 7s5p4d2f for Mn, 3s2p1d for C and O, and 3s2p for hydrogen, showed a similar composition having large 3d contributions with a knot and also substantial carbonyl π^* character. A smaller basis set with 3s2p1d for C and O gave similar results still. MRCI excitation energies with the smaller basis set give values of 30 000, 43 700, and 37 000 cm^{-1} for the A^3E, B^3A_1, and A^1A_2 states, respectively, relative to the ground state at −1 713.945 379 au. These results are from 2900 to 1800 cm^{-1} higher than those obtained with the Wachter's basis. Incidentally, the use of polarization on the carbonyl ligands (ANO basis sets from Molcas-3) does not provide any significant change in the excitation energies.

4. Discussion and Conclusion

Overall, very good reproducibility is shown, given the various methods used. The energetic results stayed essentially the same whether CASSCF MOs (generated by average over several states) or NOs (resulting from a unique CASSCF performed for a given state) were used in calculating the energy, but we would nonetheless recommend against the use of NOs in the higher excited state region. While the MRCI wave function converges faster with the CASSCF NOs, the mixed nature of the CI wave function is usually more closely approached with the MOs and it is in any case preferable for potential calculations of Rydberg states. The CASPT2 results were also in excellent agreement with the MRCI values for those cases where there is no intruder-state problem. This agreement demonstrates that the restriction to eight electrons of the number of electrons correlated with MRCI is reasonable, since virtually the same energy differences are obtained in the CASPT2 where all 66 valence electrons were correlated. Unfortunately, the severe intruder-state problems in the upper states in the case of $HMn(CO)_5$ do not allow the use of CASPT2 for the study of photodynamics. In general, using the $^5A_2$ wave function to build a contracted CI shows a slight underestimation of the vertical transition energy, which is expected, due to a likely better description of the excited states with respect to the ground state. Deviations from this trend occur for the higher states, which are highly mixed. Since the average CASSCF MOs provide wave functions that describe more closely the nondynamic correlation than those of the $^5A_2$ wave function, the former are judged to give the more reliable results.

On the basis of the new and more sophisticated calculations reported here, the assignment of the experimental spectrum of $HMn(CO)_5$ has been significantly improved. Indeed, in the previous work[4,5] only the lowest A^1E state was unambiguously assigned. While it is confirmed that this state is purely metal-centered, it is shown that the B^1E state has a mixed character and contributes to the first intense band of the spectrum. This more refined treatment of the theoretical spectrum has enabled us to exclude the presence of Rydberg states in the high-energy domain of absorption.

The following observations should be considered in future studies on related complexes: (i) an average CASSCF wave function over four or five states of a given spin and symmetry species is better for describing highly mixed excited states than a "parent" wave function optimized for each electronic state; (ii) due to the intruder state problem, the multireference CI approach with judiciously chosen active and reference space is more appropriate than a perturbation approach, especially when the degree of mixing between several electronic states is very high; (iii) the use of CASSCF natural orbitals does not appreciably improve the quality of the results and may cause some artificial localization effects; (iv) the metal 3s and 3p electron correlation has a minor contribution to the excitation energies.

The a,b^3A_1 states are not Rydberg states, as was previously suggested. In fact, the a,b^3A_1 states are both of valence character. Interestingly, it is not at all clear whether the B^1A_1 states are also valence.

On the basis of MRCI vertical excitation energies and CASSCF oscillator strengths, at least 5 transitions are determined to underlie the region between 35 000 and 55 000 cm^{-1} of the UV vapor phase spectrum. The lower band is composed predominantly of two excitations A^1E ($3d_\pi \rightarrow 3d_{x^2-y^2}$) and B^1E ($3d_\pi \rightarrow \pi^*_{CO}$ ($3b_2$)). The central band owes its intensity essentially to the $B^1A_1 \leftarrow {}^1A_1$ absorption, which is a mixture of $3d_{xy} \rightarrow \pi^*_{CO}$ ($3b_2$) and $3d_\pi \rightarrow \pi^*_{CO}$ (12e). Note, the $^1A_1 \rightarrow C^1E$ transition, having predominantly $3d_\pi,\pi^*(3b_2)$ and $3d_\pi,\sigma^*_{Mn-H}$ character, also underlies the central band, but it is relatively weak. Finally, the uppermost band is assigned to the $B^1A_1 \leftarrow {}^1A_1$ absorption. The B^1A_1 state has a significant ($\sigma_{Mn-H} \rightarrow \sigma^*_{Mn-H}$) contribution among others and is expected to lead to a broad band.

With the good vertical excitation energy coverage of the photoactive region and the qualitative agreement of oscillator strength, we believe to have identified the most likely photo-initiating states for the observed photoreactions in the near-UV of $HMn(CO)_5$. The A^1E or B^1E states are confirmed as the more likely candidates leading to the heterolytic Mn−CO dissociation. The $3d_\pi \rightarrow \pi^*_{CO}$ ($3b_2$) potential energy curve leads to the Mn−CO dissociation, while $3d_\pi \rightarrow 3d_{x^2-y^2}$ is bound.[5] For the Mn−H homolysis, the situation is much more complicated. We note that the C^1E state would not be highly populated relative to the B^1A_1 and C^1A_1 states when irradiated around 195 nm (51 300 cm^{-1}). It would thus appear reasonable to ask if an alternative mechanism through the B^1A_1 and C^1A_1 potentials could be proposed. At this point, one can only speculate as to the potential photodissociation mechanism in which these states may be involved, but it is certainly intriguing that $^1(\sigma_{Mn-H} \rightarrow \sigma^*_{Mn-H})$ corresponds to Mn−H bond weakening, although this must be weighed against the fact that this configuration dissociates into an ionic dissociation channel.

On the basis of this work, refined two-dimensional potential energy surfaces (q_a = Mn−H, q_b = Mn−CO) will be built in order to detect critical geometries (using the gradient CASSCF method) which occur along the dissociation channels. A subsequent investigation of the photodissociation dynamics will be performed with the aim of characterizing the time scale of the primary reactions, the shape of the absorption spectrum, and the efficiency of the intersystem crossing processes.

Acknowledgment. M.H. thanks the French foreign ministry for funding through the Chateaubriand fellowship. The calculations were carried out on the IBM RS 6000/390 of the Laboratoire de Chimie Quantique de Strasbourg.

IC9707523

(21) Moore, C. E. *Atomic Energy Levels*; National Bureau of Standards Circular 467; U.S. Government Printing Office: Washington, DC, 1949; Vol. II.

(22) Hall, M. B. *J. Am. Chem. Soc.* **1975**, *97*, 2057.